Radiation pressure of active dispersive chiral slabs

Maoyan Wang,[1,*] Hailong Li,[1] Dongliang Gao,[2] Lei Gao,[2] Jun Xu,[1] and Cheng-Wei Qiu[3]

[1]*School of Physical Electronics, University of Electronic Science and Technology of China, Cheng du, 610054, China*

[2]*College of Physics, Optoelectronics and Energy & Collaborative Innovation Center of Suzhou Nano Science and Technology, Soochow University, Suzhou, 215006, China*

[3]*Department of Electrical and Computer Engineering, National University of Singapore, Singapore, 119620, Singapore*

[*]*wmybrimlhl@163.com*

Abstract: We report a mechanism to obtain optical pulling or pushing forces exerted on the active dispersive chiral media. Electromagnetic wave equations for the pure chiral media using constitutive relations containing dispersive Drude models are numerically solved by means of Auxiliary Differential Equation Finite Difference Time Domain (ADE-FDTD) method. This method allows us to access the time averaged Lorentz force densities exerted on the magnetoelectric coupling chiral slabs via the derivation of bound electric and magnetic charge densities, as well as bound electric and magnetic current densities. Due to the continuously coupled cross-polarized electromagnetic waves, we find that the pressure gradient force is engendered on the active chiral slabs under a plane wave incidence. By changing the material parameters of the slabs, the total radiation pressure exerted on a single slab can be directed either along the propagation direction or in the opposite direction. This finding provides a promising avenue for detecting the chirality of materials by optical forces.

OCIS codes: (260.2110) Electromagnetic optics; (260.2030) Dispersion.

References and links

1. I. V. Lindell, A. H. Sihvola, S. A. Tretyakov, and A. J. Viitanen, *Electromagnetic Waves in Chiral and Bi-isotropic Media* (Artech House, 1994).
2. W. Y. Tsai, J. S. Huang, and C. B. Huang, "Selective trapping or rotation of isotropic dielectric microparticles by optical near field in a plasmonic archimedes spiral," Nano Lett. **14**(2), 547–552 (2014).
3. K. Ding, J. Ng, L. Zhou, and C. T. Chan, "Realization of optical pulling forces using chirality," Phys. Rev. A **89**(6), 063825 (2014).
4. R. Zhao, J. Zhou, T. Koschny, E. N. Economou, and C. M. Soukoulis, "Repulsive Casimir force in chiral metamaterials," Phys. Rev. Lett. **103**(10), 103602 (2009).
5. Q. C. Shang, Z. S. Wu, T. Qu, Z. J. Li, L. Bai, and L. Gong, "Analysis of the radiation force and torque exerted on a chiral sphere by a Gaussian beam," Opt. Express **21**(7), 8677–8688 (2013).
6. J. Durnin, J. Miceli, Jr., and J. H. Eberly, "Diffraction-free beams," Phys. Rev. Lett. **58**(15), 1499–1501 (1987).
7. M. Fujii, "Finite-difference analysis of plasmon-induced forces of metal nano-clusters by the Lorentz force formulation," Opt. Express **18**(26), 27731–27747 (2010).
8. T. Cižmár, V. Kollárová, X. Tsampoula, F. Gunn-Moore, W. Sibbett, Z. Bouchal, and K. Dholakia, "Generation of multiple Bessel beams for a biophotonics workstation," Opt. Express **16**(18), 14024–14035 (2008).
9. A. Ashkin, J. M. Dziedzic, J. E. Bjorkholm, and S. Chu, "Observation of a single-beam gradient force optical trap for dielectric particles," Opt. Lett. **11**(5), 288–290 (1986).
10. J. M. Auñón and M. Nieto-Vesperinas, "Partially coherent fluctuating sources that produce the same optical force as a laser beam," Opt. Lett. **38**(15), 2869–2872 (2013).
11. D. Gao, C. W. Qiu, L. Gao, T. Cui, and S. Zhang, "Macroscopic broadband optical escalator with force-loaded transformation optics," Opt. Express **21**(1), 796–803 (2013).
12. S. H. Lee, Y. Roichman, and D. G. Grier, "Optical solenoid beams," Opt. Express **18**(7), 6988–6993 (2010).
13. I. V. Krasnov, "Bichromatic optical tractor beam for resonant atoms," Phys. Lett. A **376**(42–43), 2743–2749 (2012).
14. A. Mizrahi and Y. Fainman, "Negative radiation pressure on gain medium structures," Opt. Lett. **35**(20), 3405–3407 (2010).

#237657 Received 7 Apr 2015; revised 10 Jun 2015; accepted 11 Jun 2015; published 15 Jun 2015

15. A. Akbarzadeh, M. Danesh, C. W. Qiu, and A. J. Danner, "Tracing optical force fields within graded-index media," New J. Phys. **16**(5), 053035 (2014).
16. A. Novitsky and C. W. Qiu, "Pulling extremely anisotropic lossy particles using light without intensity gradient," Phys. Rev. A **90**(5), 053815 (2014).
17. Y. Nishijima, L. Rosa, and S. Juodkazis, "Long-range interaction of localized surface plasmons in periodic and random patterns of Au nanoparticles," Appl. Phys., A Mater. Sci. Process. **115**(2), 409–414 (2014).
18. A. Salandrino and D. N. Christodoulides, "Reverse optical forces in negative index dielectric waveguide arrays," Opt. Lett. **36**(16), 3103–3105 (2011).
19. K. J. Webb and Shivanand, "Negative electromagnetic plane-wave force in gain media," Phys. Rev. E Stat. Nonlin. Soft Matter Phys. **84**(5 5 Pt 2), 057602 (2011).
20. V. Kajorndejnukul, W. Q. Ding, S. Sukhov, C. W. Qiu, and A. Dogariu, "Linear momentum increase and negative optical forces at dielectric interface," Nat. Photonics **7**(10), 787–790 (2013).
21. D. S. Bradshaw and D. L. Andrews, "Chiral discrimination in optical trapping and manipulation," New J. Phys. **16**(10), 103021 (2014).
22. A. Di Falco, "Chiral plasmonic nanostructures: twisted by DNA," Nat. Mater. **13**(9), 846–848 (2014).
23. J. A. Pereda, A. Grande, O. González, and Á. Vegas, "FDTD modeling of chiral media by using the mobius transformation technique," IEEE Antenn. Wirel. Prop. Lett. **5**(1), 327–330 (2006).
24. V. Demir, A. Z. Elsherbeni, and E. Arvas, "FDTD formulation for dispersive chiral media using the Z transform method," IEEE Trans. Antenn. Propag. **53**(10), 3374–3384 (2005).
25. A. Sihvola, "Metamaterials in electromagnetics," Metamaterials (Amst.) **1**(1), 2–11 (2007).
26. S. Tretyakov, I. Nefedov, A. Sihvola, S. Maslovski, and C. Simovski, "Waves and energy in chiral nihility," J. Electromagn. Wave **17**(5), 695–706 (2003).
27. A. R. Zakharian, P. Polynkin, M. Mansuripur, and J. V. Moloney, "Single-beam trapping of micro-beads in polarized light: numerical simulations," Opt. Express **14**(8), 3660–3676 (2006).
28. A. Zakharian, M. Mansuripur, and J. Moloney, "Radiation pressure and the distribution of electromagnetic force in dielectric media," Opt. Express **13**(7), 2321–2336 (2005).
29. J. Q. Qin, X. L. Wang, D. Jia, J. Chen, Y. X. Fan, J. Ding, and H. T. Wang, "FDTD approach to optical forces of tightly focused vector beams on metal particles," Opt. Express **17**(10), 8407–8416 (2009).
30. A. Akyurtlu and D. H. Werner, "BI-FDTD: a novel Finite-Difference Time-Domain formulation for modeling wave propagation in Bi-isotropic media," IEEE Trans. Antenn. Propag. **52**(2), 416–425 (2004).
31. A. Grande, I. Barba, A. C. L. Cabeceira, J. Represa, K. Kärkkäinen, and A. H. Sihvola, "Two-dimensional extension of a novel FDTD technique for modeling dispersive lossy Bi-isotropic media using the auxiliary differential equation method," IEEE Microw. Wirel. Compon. Lett. **15**(5), 375–377 (2005).
32. N. Engheta and R. W. Ziolkowski, "A positive future for double-negative metamaterials," IEEE Trans. Microw. Theory Tech. **53**(4), 1535–1556 (2005).
33. A. Taflove and S. C. Hagness, *Computational Electrodynamics: the Finite-Difference Time-Domain Method* (Artech House, 2005).
34. I. V. Semchenko, S. A. Tretyakov, and A. N. Serdyukov, "Research on chiral and bianisotropic media in Byelorussia and Russia in the last ten years," Prog. Electromagnetics Res. **12**, 335–370 (1996).
35. B. Kemp, T. Grzegorczyk, and J. Kong, "Ab initio study of the radiation pressure on dielectric and magnetic media," Opt. Express **13**(23), 9280–9291 (2005).
36. G. Tkachenko and E. Brasselet, "Helicity-dependent three-dimensional optical trapping of chiral microparticles," Nat. Commun. **5**, 4491 (2014).
37. H. P. Xiao, C. Y. He, C. X. Zhang, L. Z. Sun, P. Zhou, and J. X. Zhong, "Stability, electronic structures and transport properties of armchair (10, 10) BN/C nanotubes," J. Solid State Chem. **200**, 294–298 (2013).
38. H. Liu, D. Nishide, T. Tanaka, and H. Kataura, "Large-scale single-chirality separation of single-wall carbon nanotubes by simple gel chromatography," Nat. Commun. **2**, 309 (2011).
39. V. V. Pokropivny, "Noncarbon nanotubes, synthesis, structure, properties and promising applications," in *Proceedings of the 2001 International Conference Hydrogen Materials Science and Chemistry of Metal Hydrides*, D. V. Schur, S. Y. Zaginaichenko, eds. (Springer, 2001), pp. 630–631.
40. T. Kawasaki, M. Nakaoda, Y. Takahashi, Y. Kanto, N. Kuruhara, K. Hosoi, I. Sato, A. Matsumoto, and K. Soai, "Self-replication and amplification of enantiomeric excess of chiral multifunctionalized large molecules by asymmetric autocatalysis," Angew. Chem. Int. Ed. **126**(42), 11381–11384 (2014).
41. B. N. Wang, J. F. Zhou, T. Koschny, M. Kafesaki, and C. M. Soukoulis, "Chiral metamaterials: simulations and experiments," J. Opt. A, Pure Appl. Opt. **11**(11), 114003 (2009).
42. K. Hannam, D. A. Powell, I. V. Shadrivov, and Y. S. Kivshar, "Broadband chiral metamaterials with large optical activity," Phys. Rev. B **89**(12), 125105 (2014).
43. M. Mansuripur, "On the foundational equations of the classical theory of electrodynamics," Resonance **18**(2), 130–155 (2013).

1. Introduction

Optical pulling forces have attracted considerable attention due to its potential applications in physical, biological, chemical and mechanical sciences [1–20]. The negative optical forces can be achieved by the configuration of optical fields, such as diffraction-free Bessel beams [6–8], optical solenoid beams [12], bichromatic fields [13] etc. Moreover, optical pulling forces exerted on gain medium structures [14,19], graded-index media [15], nonmagnetic

#237657 Received 7 Apr 2015; revised 10 Jun 2015; accepted 11 Jun 2015; published 15 Jun 2015

anisotropic beads [16], and chiral structures [1–4] have been studied recently. In [14], Mizrahi et al. present negative radiation pressure on media with the negative imaginary part of permittivity. Lindell et al. [1] demonstrate the trapping of micro-particles in a single gold plasmonic Archimedes spiral and Ding et al. [3] analytically show 25 metallic spheres arranged in a spiral to realize an optical pulling force. Nevertheless, the complicated mechanism of optical Lorentz forces acting on chiral media requires further research.

Chiral media [1–5, 21–42] have the properties of giant optical rotation and circular dichroism. In terms of structure, there are three general types of chiral media. They are namely: pure chiral medium equivalent to dispersive material, artificial chiral medium composed of helices etc., and natural chiral medium, such as DNA molecules. Although most natural and artificial chiral materials are passive, Boron Nitride NanoTubes [37,38], whose tube chirality distribution is determined by electron diffraction, are predicted to be used as gain media for phonons generation [39]. Besides the chiral multifunctionalized large molecules [40] and chiral metamaterials [41,42] with large optical rotation are potential active chiral materials. Lindell analyzes how pure chiral media affect electromagnetic fields and wave propagation [1]. Tretyakov and Sihvola et al. discuss waves and energy in chiral nihility with zero permittivity and permeability [26]. The effective permittivity, permeability, and chirality of chiral media [1,24] must be frequency-dispersive to satisfy the interaction between electromagnetic fields and a resonant chiral particle.

However, available optical force for pure chiral media has not been reported yet. The Maxwell stress tensor approach and direct application of the Lorentz force are common methods to compute the optical force by using the electromagnetic field distributions of particles. Radiation pressure and the distribution of electromagnetic force in effective electric dispersive or magnetic dispersive achiral media are discussed [28,35].

Furthermore, the Finite-difference time-domain (FDTD) method, as a popular numerical electromagnetic computational analysis technique [29–33], can study any kind of chiral media. The BI-FDTD method [30,31] based on wave decomposition technique [5] is valid only as the wavefields in chiral media remain uncoupled. Some FDTD methods are based on a direct implementation of the magnetoelectric coupling chiral constitutive relations into Maxwell's equations. Z-transform [24], Auxiliary Differential Equation (ADE) [31], Recursive Convolution, and Shift Operator techniques are generally used to simulate dispersive media. Considering the complex constitutive relations for chiral media, the ADE-FDTD method is given to simulate the dispersive chiral media.

In this paper, the distribution of Lorentz force densities in active dispersive chiral slabs is studied by using the ADE-FDTD method. First, wave equations for chiral media are given by introducing the frequency-dependent permittivity, permeability, and chiral parameter. Then, the Lorentz force for dispersive and magnetoelectric coupling chiral media is developed and incorporated by the FDTD method. Validations of algorithms and programs are performed by comparing with theoretical results of the radiation pressure in [28], for a given set of parameter values. The positive or negative radiation pressure acting on active chiral slabs is investigated.

2. Theory

2.1 Constitute relation for chiral media

The constitutive relations that describe magnetoelectric coupling for generally bi-isotropic media in the frequency domain can be expressed in the following form [1],

$$\boldsymbol{D}(\omega) = \varepsilon(\omega)\boldsymbol{E} + \left[\chi(\omega) - \mathrm{j}\kappa(\omega)\right]\sqrt{\mu_0\varepsilon_0}\boldsymbol{H}, \tag{1}$$

$$\boldsymbol{B}(\omega) = \mu(\omega)\boldsymbol{H} + \left[\chi(\omega) + \mathrm{j}\kappa(\omega)\right]\sqrt{\mu_0\varepsilon_0}\boldsymbol{E}, \tag{2}$$

where the time harmonic convention $e^{\mathrm{j}\omega t}$ is assumed. $\varepsilon(\omega)$, $\mu(\omega)$, $\chi(\omega)$, and $\kappa(\omega)$ represent frequency-dispersive permittivity, permeability, Tellegen, and chirality parameter,

#237657 Received 7 Apr 2015; revised 10 Jun 2015; accepted 11 Jun 2015; published 15 Jun 2015

respectively. The macroscopic and effective material parameters of chiral media [36–42] are controlled by the physical geometric structure, material, angle of incidence, and so on. A purely chiral medium is discussed in this paper, in which case $\chi = 0$.

In view of the complications and spatial dispersion of Lorentz and Condon models [23], the lossy Drude models are used to characterize the permittivity, permeability, and chirality parameter for chiral media as [34]

$$\varepsilon(\omega) = \varepsilon_\infty \varepsilon_0 - \frac{\varepsilon_0 \omega_{pe}^2}{\omega(\omega - \mathrm{j}\Gamma_e)}, \quad \mu(\omega) = \mu_\infty \mu_0 - \frac{\mu_0 \omega_{pm}^2}{\omega(\omega - \mathrm{j}\Gamma_m)}, \quad \mathrm{j}\kappa(\omega) = \frac{\omega_{p\kappa}^2}{\omega(\omega - \mathrm{j}\Gamma_\kappa)}, \tag{3}$$

where ω_{pe}, ω_{pm}, $\omega_{p\kappa}$, Γ_e, Γ_m, and Γ_κ are the electric, magnetic, and magnetoelectric coupling plasma frequency and relaxation rate, respectively.

Conditions for the material parameters of a passive chiral medium are [1]

$$\mathrm{Im}\{\mu\} < 0, \quad \mathrm{Im}\{\varepsilon\} < 0, \quad \mathrm{Im}^2\{\kappa\} < \frac{\mathrm{Im}\{\mu\}\,\mathrm{Im}\{\varepsilon\}}{\mu_0 \varepsilon_0}. \tag{4}$$

Otherwise, the chiral medium would be an active medium [24].

By substituting Eq. (3) into Eq. (4), one can obtain

$$\frac{-\omega\omega_{pe}^2\Gamma_e}{\omega^4 + \omega^2\Gamma_e^2} < 0, \quad \frac{-\omega\omega_{pm}^2\Gamma_m}{\omega^4 + \omega^2\Gamma_m^2} < 0, \quad \left(\frac{\omega^2\omega_{p\kappa}^2}{\omega^4 + \omega^2\Gamma_\kappa^2}\right)^2 < \frac{\omega\omega_{pe}^2\Gamma_e}{\omega^4 + \omega^2\Gamma_e^2} \cdot \frac{\omega\omega_{pm}^2\Gamma_m}{\omega^4 + \omega^2\Gamma_m^2}. \tag{5}$$

As all the material parameters are positive, the former two conditions for passive chiral media in Eq. (5) are automatically satisfied. A function used to determine whether the medium is active can be defined by

$$S = \frac{\omega\omega_{pe}^2\Gamma_e}{\omega^4 + \omega^2\Gamma_e^2} \cdot \frac{\omega\omega_{pm}^2\Gamma_m}{\omega^4 + \omega^2\Gamma_m^2} - \left(\frac{\omega^2\omega_{p\kappa}^2}{\omega^4 + \omega^2\Gamma_\kappa^2}\right)^2. \tag{6}$$

If the value of S is larger than zero, the chiral medium is active; if the value of S is smaller than zero, the chiral medium is passive.

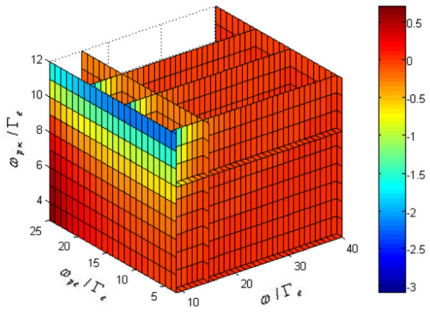

Fig. 1. Function S versus electric plasma frequency, magnetoelectric coupling plasma frequency, and working frequency normalized by electric relaxation rate.

By setting some of the material parameters for chiral media to be $\Gamma_e = \Gamma_m = \Gamma_\kappa$, and $\omega_{pe} = \omega_{pm}$, the function S depending on the material parameters and working frequency is illustrated in Fig. 1. Generally speaking, the function S decreases as the magnetoelectric coupling plasma frequency $\omega_{p\kappa}$ increases, as well as the electric plasma frequency ω_{pe} and working frequency ω decrease.

#237657 Received 7 Apr 2015; revised 10 Jun 2015; accepted 11 Jun 2015; published 15 Jun 2015

2.2 Wave equations of the ADE-FDTD method for chiral media

Assuming $\chi = 0$, the corresponding induced electric current $\boldsymbol{J}$ and coupled magnetic current $\boldsymbol{K}_c$ in chiral media are expressed as

$$\frac{\boldsymbol{J}}{\mathrm{j}\omega} = \frac{\varepsilon_0 \omega_{pe}^2 \boldsymbol{E}}{(\mathrm{j}\omega)^2 + \Gamma_e(\mathrm{j}\omega)} = \boldsymbol{P}_e, \quad \frac{\boldsymbol{K}_c}{\mathrm{j}\omega} = \frac{\omega_{p\kappa}^2 \sqrt{\mu_0 \varepsilon_0}\boldsymbol{H}}{(\mathrm{j}\omega)^2 + \Gamma_\kappa(\mathrm{j}\omega)} = \boldsymbol{M}_c. \tag{7}$$

In Eq. (7), the electric polarization $\boldsymbol{P}_e$ and the coupled magnetic polarization $\boldsymbol{M}_c$ are related to the electric current $\boldsymbol{J}$ and magnetic current $\boldsymbol{K}_c$.

Similarly, the corresponding relation between the magnetic polarization $\boldsymbol{M}_n$ and the magnetic current $\boldsymbol{K}$ in addition to the relation between the coupled electric polarization $\boldsymbol{P}_c$ and the electric current $\boldsymbol{J}_c$ in the frequency domain are

$$\frac{\boldsymbol{K}}{\mathrm{j}\omega} = \frac{\mu_0 \omega_{pm}^2 \boldsymbol{H}}{(\mathrm{j}\omega)^2 + \Gamma_m(\mathrm{j}\omega)} = \boldsymbol{M}_n, \quad \frac{\boldsymbol{J}_c}{\mathrm{j}\omega} = \frac{-\omega_{p\kappa}^2 \sqrt{\mu_0 \varepsilon_0}\boldsymbol{E}}{(\mathrm{j}\omega)^2 + \Gamma_\kappa(\mathrm{j}\omega)} = \boldsymbol{P}_c. \tag{8}$$

By using the transform relation between frequency domain and time domain $\mathrm{j}\omega \to \partial/\partial t$, the electromagnetic field and current equations used to model the waves in a chiral medium become

$$\begin{aligned} \nabla \times \boldsymbol{H} &= \varepsilon_\infty \varepsilon_0 \partial \boldsymbol{E} / \partial t + \boldsymbol{J} + \boldsymbol{J}_s + \boldsymbol{K}_c, \quad \nabla \times \boldsymbol{E} = -\mu_\infty \mu_0 \partial \boldsymbol{H} / \partial t - \boldsymbol{K} - \boldsymbol{J}_c, \\ \partial \boldsymbol{J} / \partial t + \Gamma_e \boldsymbol{J} &= \varepsilon_0 \omega_{pe}^2 \boldsymbol{E}, \qquad \partial \boldsymbol{K} / \partial t + \Gamma_m \boldsymbol{K} = \mu_0 \omega_{pm}^2 \mathbf{H}, \\ \partial \boldsymbol{K}_c / \partial t + \Gamma_\kappa \boldsymbol{K}_c &= \sqrt{\varepsilon_0 \mu_0}\, \omega_{p\kappa}^2 \boldsymbol{H}, \qquad \partial \boldsymbol{J}_c / \partial t + \Gamma_\kappa \boldsymbol{J}_c = -\sqrt{\varepsilon_0 \mu_0}\, \omega_{p\kappa}^2 \boldsymbol{E}. \end{aligned} \tag{9}$$

The update equations for co- and cross-polarized components of fields and currents can be obtained by discretizing Eq. (9) in the form of a Yee cell. For one dimensional problems, only *x*- and *y*-components of electromagnetic fields are kept in the recurrence equations of the FDTD method if $\partial/\partial x = 0$ and $\partial/\partial y = 0$. The fields E_x and H_y are the components of incident co-polarized light, whereas E_y and H_x are the components of induced cross-polarized light.

2.3 Lorentz force density exerted by electromagnetic fields on chiral media

According to the Lorentz force law, the generalized and equivalent formula of Lorentz force density resulting from radiation pressure is [43]

$$\boldsymbol{F}(\boldsymbol{r}, t) = (\boldsymbol{J}_{\text{free}} + \partial \boldsymbol{P} / \partial t) \times \mu_0 \boldsymbol{H} + (\rho_{\text{free}} - \nabla \cdot \boldsymbol{P})\boldsymbol{E} - (\nabla \cdot \boldsymbol{M})\boldsymbol{H} - (\partial \boldsymbol{M} / \partial t) \times \varepsilon_0 \boldsymbol{E}, \tag{10}$$

where ρ_{free} and J_{free} are free charge and free current sources.

The electric displacement $\boldsymbol{D}$ and magnetic induction $\boldsymbol{B}$ for dispersive chiral media in Eqs. (1) and (2) can be rewritten as

$$\boldsymbol{D} = \varepsilon_0 \boldsymbol{E} + \boldsymbol{P} = \varepsilon_\infty \varepsilon_0 \boldsymbol{E} + (\boldsymbol{P}_e + \boldsymbol{M}_c), \quad \boldsymbol{B} = \mu_0 \boldsymbol{H} + \boldsymbol{M} = \mu_\infty \mu_0 \boldsymbol{H} + (\boldsymbol{M}_n + \boldsymbol{P}_c). \tag{11}$$

Then, the bound electric charge density $\rho_{\text{e\_bound}}$, bound electric current density $J_{\text{e\_bound}}$, bound magnetic charge density $\rho_{\text{m\_bound}}$, and current density $J_{\text{m\_bound}}$ based on the Maxwell equations for chiral media can be presented as

$$\begin{aligned} \rho_{\text{e\_bound}} &= \varepsilon_0 \nabla \cdot \boldsymbol{E} = -\nabla \cdot \boldsymbol{P}, \quad \rho_{\text{m\_bound}} = \mu_0 \nabla \cdot \boldsymbol{H} = -\nabla \cdot \boldsymbol{M}, \\ \boldsymbol{J}_{\text{e\_bound}} &= \partial \boldsymbol{P} / \partial t = [\partial(\boldsymbol{P}_e + \boldsymbol{M}_c) / \partial t + (\varepsilon_\infty - 1)(\nabla \times \boldsymbol{H})] / \varepsilon_\infty, \\ \boldsymbol{J}_{\text{m\_bound}} &= \partial \boldsymbol{M} / \partial t = [\partial(\boldsymbol{M}_n + \boldsymbol{P}_c) / \partial t + (1 - \mu_\infty) \nabla \times \boldsymbol{E}] / \mu_\infty. \end{aligned} \tag{12}$$

Given the electromagnetic fields, charges, and currents as functions of time and spatial coordinates, the time averaged Lorentz force density for chiral media without free charge and current sources is

#237657 Received 7 Apr 2015; revised 10 Jun 2015; accepted 11 Jun 2015; published 15 Jun 2015

$$< \boldsymbol{F} >= (1/T)\int_0^T (\rho_{\text{e\_bound}}\boldsymbol{E} + \boldsymbol{J}_{\text{e\_bound}} \times \mu_0 \boldsymbol{H} + \rho_{\text{m\_bound}}\boldsymbol{H} - \boldsymbol{J}_{\text{m\_bound}} \times \varepsilon_0 \boldsymbol{E})dt. \qquad (13)$$

The time integral in Eq. (13) can be taken over one period of the stable time harmonic electromagnetic fields. Due to circular dichroism of chiral media, the forces for co- and cross-polarization are different from those for the orthogonal polarization states of fields.

3. Numerical results

To validate the algorithms and programs, the time averaged Lorentz force density of a 110 nm-thickness dielectric slab with $\varepsilon_r = 4$ in free space is simulated. The working wavelength and $\boldsymbol{E}$-field amplitude of the normally incident sine plane wave along $-z$-axis are $\lambda_0 = 640$ nm and $E_0 = 1.0$ V/m respectively. Taking reference to the numerical result of –2.481 pN/m^2 and the exact value of –2.479 pN/m^2 in [28], the computed total radiation pressure in this paper is $\int F_z(z)\mathrm{d}z = -2.4188$ pN/m^2. The relative error is less than 0.025 with respect to the exact value in [28]. The error is caused by the different treatments of material parameter, field and force discontinuities at material interfaces; a similar case can be found in a semi-infinite dielectric example discussed in [28]. The average $\boldsymbol{E}$ across the boundary, ½($\boldsymbol{E}_{1\perp}$ + $\boldsymbol{E}_{2\perp}$), is used in calculating the interfacial force in [28]; however, the average (effective) medium parameters [33], rather than the average $\boldsymbol{E}$, across the boundary are used in calculating the interfacial electromagnetic fields and forces in this paper. Such transitions of smooth medium parameters at the interfaces have been proved effective in simulating physical reality, as well as eliminating sharp singularities and discontinuities of the Maxwell and Lorentz force equations [28,33].

3.1 Radiation pressure exerted on a single chiral slab

Artificial chiral media are generally composed of periodically arranged elemental unit cells; in addition, natural chiral architectures usually consist of large chiral molecules. The optical forces acting on such units or their aggregates are not well known. In order to explore the mutual Lorentz force between the chiral units, the radiation pressure acting on two chiral slabs are displayed in this section.

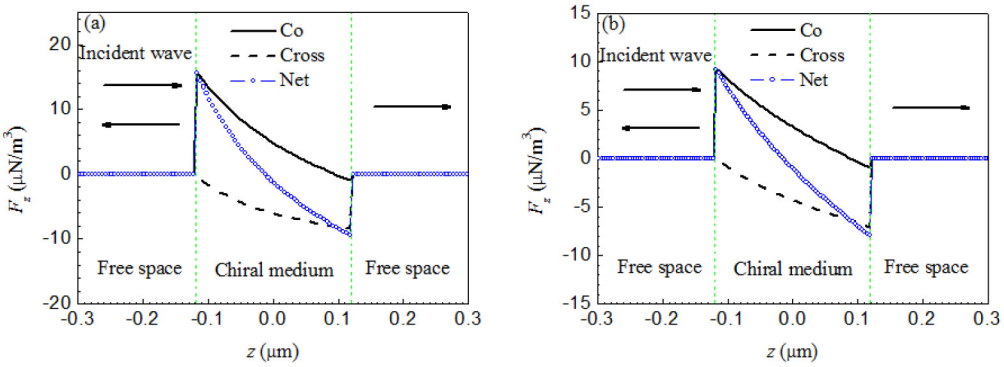

Fig. 2. FDTD predicted co-polarized, cross-polarized, and net force densities F_z of a chiral slab suspended in free space. (a) $\lambda_0 = 640$ nm, (b) $\lambda_0 = 480$ nm.

Figure 2 compares co-polarized, cross-polarized, and net Lorentz force densities (per unit cross-sectional area) of a 240 nm-thickness chiral slab (marked by the green dashed lines) illuminated by plane waves of wavelength $\lambda_0 = 640$ nm and $\lambda_0 = 480$ nm at normal incidence, respectively. The slab is assumed to be parallel to the xy-plane and the waves propagate in the z-direction. If not specially specified in this paper, the amplitude of incident electric field is chosen to $E_0 = 1.0$ V/m, the FDTD cell size $\delta = \lambda_0/128$, and time step $\Delta t = \delta/2c$. All medium parameters across the interface are the mean value of media parameters for two adjacent media.

#237657 Received 7 Apr 2015; revised 10 Jun 2015; accepted 11 Jun 2015; published 15 Jun 2015

The material parameters for the chiral slab are $\varepsilon_\infty = \mu_\infty = 1$, $\omega_{pe} = \omega_{pm} = 2\pi \times 600$ THz, $\omega_{p\kappa} = 2\pi \times 264.58$ THz, $\Gamma_e = \Gamma_m = 300$ THz, $\Gamma_\kappa = 200$ THz. The values of relative permittivity ε_r, permeability μ_r, and chiral parameter κ_r at $\lambda_0 = 640$ nm are –0.62–j0.17, –0.62–j0.17, and –0.02–j0.32, respectively. The values of ε_r, μ_r, and κ_r at $\lambda_0 = 480$ nm are 0.08–j0.07, 0.08–j0.07, and –0.009–j0.18. Because of $\varepsilon_0\mu_0\mathrm{Im}^2\{\kappa\} > \mathrm{Im}\{\mu\}\mathrm{Im}\{\varepsilon\}$, the chiral media discussed in this paper are gain media, which are different from gain medium structures having negative imaginary part of permittivity or permeability [14,19]. Whereas the absolute values of cross-polarized and net force densities keep increasing in Fig. 2, the positive co-polarized force density F_z decreases and becomes negative as the plane wave propagates into the active chiral slab. The total co-polarized, cross-polarized, and net radiation pressure along the + z-axis by integrating the various local force densities across the chiral slab are $\int F_{\mathrm{co}}(z)\mathrm{d}z = 1.37$ pN/m^2, $\int F_{\mathrm{cr}}(z)\mathrm{d}z = -1.32$ pN/m^2, $\int F_{\mathrm{net}}(z)\mathrm{d}z = 0.05$ pN/m^2, and $\int F_{\mathrm{co}}(z)\mathrm{d}z = 0.85$ pN/m^2, $\int F_{\mathrm{cr}}(z)\mathrm{d}z = -0.97$ pN/m^2, $\int F_{\mathrm{net}}(z)\mathrm{d}z = -0.12$ pN/m^2 in Figs. 2(a) and 2(b), respectively. For a one-dimensional case, there are no induced bound electric and magnetic charges at normal incidence. The radiation pressure is attributed to the bound electric and magnetic currents in the chiral slab. Due to the optical rotation of the chiral medium, co-polarized electromagnetic waves are continuously coupled into cross-polarized waves as plane waves propagate into the active chiral slab. Thus, the pressure gradient force is engendered with the steady increase of cross-polarized electromagnetic waves to pull the slab towards the incident wave source. The positive or negative radiation pressure is exerted on the same chiral slab illuminated by time-harmonic plane waves, which have different working frequencies. If the thickness of the active chiral slab increases, the positive radiation pressure in Fig. 2(a) will turn into negative as the working wavelength is $\lambda_0 = 640$ nm.

3.2 Positive or negative radiation pressure acting on chiral slabs

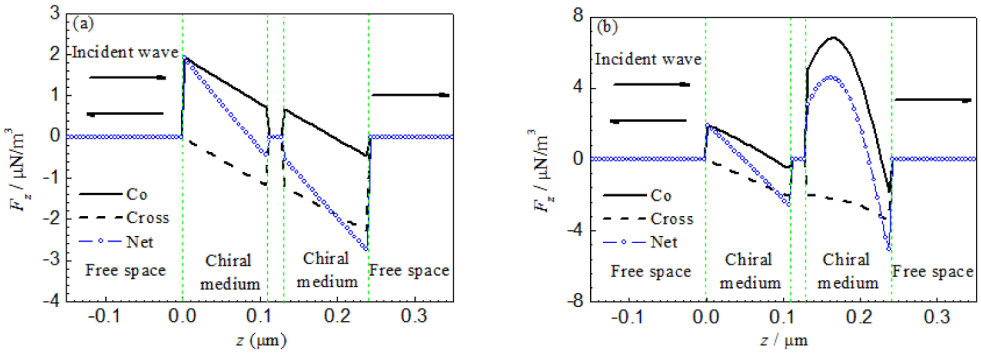

Fig. 3. Computed co-polarized, cross-polarized, and net force densities versus z inside chiral slabs. (a) pulling force densities, (b) pushing force densities.

Figure 3 presents the time averaged co-polarized, cross-polarized, and net force densities in two 110 nm-thickness and 20 nm-apart active chiral slabs under a plane wave ($\lambda_0 = 640$ nm) incidence. The material parameters for the two chiral slabs in Fig. 3(a) are $\varepsilon_\infty = \mu_\infty = 1$, $\omega_{pe} = 2\pi \times 220$ THz, $\omega_{pm} = 2\pi \times 210$ THz, $\omega_{p\kappa} = 2\pi \times 160$ THz, $\Gamma_e = \Gamma_m = 300$ THz, $\Gamma_\kappa = 200$ THz, $\varepsilon_r = 0.78–j0.02$, $\mu_r = 0.8–j0.02$, $\kappa_r = –0.008–j0.12$. The total co-polarized, cross-polarized, and net force densities along the z-axis for the first chiral slab are 0.16 pN/m^2, –0.07 pN/m^2, and 0.09 pN/m^2 and for the second chiral slab are 0.02 pN/m^2, –0.19 pN/m^2, –0.17 pN/m^2. The positive radiation pressure is imposed on the first chiral slab, whereas the negative radiation pressure is exerted on the second chiral slab. The mutual Lorentz force between the chiral slabs is a pulling force. The force densities in free space are zero. In Fig. 3(a), the force densities at the back face of the first chiral slab and the front face of the second chiral slab are somewhat continuous. Positive, negative even zero radiation pressure can be obtained by adjusting the thickness and material parameters of the chiral slabs.

#237657 Received 7 Apr 2015; revised 10 Jun 2015; accepted 11 Jun 2015; published 15 Jun 2015

In Fig. 3(b), the material parameters for the first chiral slab are $\varepsilon_\infty = \mu_\infty = 1$, $\omega_{pe} = 2\pi \times 150$ THz, $\omega_{pm} = 2\pi \times 190$ THz, $\omega_{p\kappa} = 2\pi \times 180$ THz, $\Gamma_e = \Gamma_m = 300$ THz, $\Gamma_\kappa = 100$ THz, $\varepsilon_r = 0.9$–j0.01, $\mu_r = 0.84$–j0.02, $\kappa_r = -0.005$–j0.15 and the second chiral slab are $\varepsilon_\infty = 1.69$, $\mu_\infty = 1$, $\omega_{pe} = 2\pi \times 150$ THz, $\omega_{pm} = 2\pi \times 190$ THz, $\omega_{p\kappa} = 2\pi \times 180$ THz, $\Gamma_e = \Gamma_m = 300$ THz, $\Gamma_\kappa = 100$ THz, $\varepsilon_r = 1.59$–j0.01, $\mu_r = 0.84$–j0.02, $\kappa_r = -0.005$–j0.15. The total co-polarized, cross-polarized, and net radiation pressure along the z-axis for the first chiral slab are –0.11 pN/m^2, –0.12 pN/m^2, –0.23 pN/m^2 and for the second chiral slab are 0.58 pN/m^2, –0.28 pN/m^2, and 0.3 pN/m^2. The mutual Lorentz force between the chiral slabs is a pushing force. Because the cross-polarized reflection waves are very small, the continuity of cross-polarized force densities of the two chiral slabs is barely affected by the alteration of the relative permittivity. However, the alteration greatly changes the continuity of the co-polarized force density at the front face of the second chiral slab. It is the relatively large impedance mismatch between free space and the second chiral slab that causes the increase of co-polarized reflection waves. The positive radiation pressure on the second chiral slab becomes negative as the co-polarized reflection waves are much smaller, if we reduce the thickness of the second chiral slab from 110nm to 15 nm.

4. Conclusion

The mechanical interaction between plane waves and active dispersive chiral slabs is investigated by integrating the ADE-FDTD method into the Lorentz force in this paper. Given the frequency-dependent and magnetoelectric coupling constitute relation for chiral media, the theory of the Lorentz force is developed. In addition to bound electric and magnetic charges densities, bound electric and magnetic currents densities are extended to compute the time averaged Lorentz force densities. It should be noted that the effective bound electric current arises from the induced electric polarization $\boldsymbol{P}_e$ and the coupled magnetic polarization $\boldsymbol{M}_c$, simultaneously, the effective bound magnetic current gives rise to the magnetic polarization $\boldsymbol{M}_n$ and the coupled electric polarization $\boldsymbol{P}_c$ in chiral media. Force density projections along the propagation direction for two different polarization states of electromagnetic waves are presented. We find that the pressure gradient force is generated as the cross-polarized waves are continuously coupled out by the chiral slabs. The positive or negative radiation pressure between two chiral slabs affected by material parameters and working frequency is discussed. The reported findings are believed to provide guidelines for chiral media's potential applications in optical micromanipulation.

Acknowledgments

The authors gratefully acknowledge by National University of Singapore the Grant R-263-000-678-133 administered, the National Natural Science Foundation of China under grants 41304119 and 41104097, the Specialized Research Fund for the Doctoral Program of Higher Education under grant 20120185120012, the Oversea Academic Training Fund sponsored by China Scholarship Council and University of Electronic Science and Technology of China under grant 201306075027.

#237657 Received 7 Apr 2015; revised 10 Jun 2015; accepted 11 Jun 2015; published 15 Jun 2015